JMEPEG (2019) 28:3966–3973
https://doi.org/10.1007/s11665-019-04040-z

1059-9495/$19.00

Quality Assessment of Al Castings Produced in Sand Molds Using Image and CT Analyses

Lenka Kuchariková, Eva Tillová, Michaela Samardžiová, Milan Uhríčik, Juraj Belan, and Ivana Švecová

(Submitted October 12, 2018; in revised form March 29, 2019; published online May 3, 2019)

Nowadays, the economic production of aluminum casts is becoming increasingly important. Therefore, the decision of whether to use alloys based on the primary aluminum (low Fe content, but high costs) or the secondary aluminum (high Fe content, but reasonable costs) for a cast product is a common problem. The main expected influence of higher iron content is to increase porosity and decrease mechanical and fatigue properties. Therefore, this work is focused on assessment of the higher Fe content influence on porosity and iron-rich intermetallic phases formation and, hence, changes in the mechanical properties, with simultaneously keeping the production economical. The quality of castings was measured by application of the 2D technology (image analysis) and the 3D technology (CT analysis), as well. Results show that technologies of assessment are comparable and length of the Fe-rich phases is not critical for mechanical properties, but it is important for porosity formation in materials with the higher amount of Fe.

Keywords aluminum cast alloys, computed tomography, Fe-rich needlelike intermetallic phases, image analysis, mechanical properties, porosity, sand castings

1. Introduction

The automotive and aerospace industries put a lot of attention toward aluminum alloys instead of heavy steel or cast iron application in structures (Ref 1, 2). Properties of aluminum cast alloys, such as good corrosion resistance, high strength-to-weight ratio, good formability, good machinability and scrap reuse, are great advantages for using such materials for industrial applications (Ref 1-6).

The scrap reuse for the production of the secondary aluminum alloys comes with many benefits: environmental friendly, inexpensive and low energy consumption. Aluminum alloys are considered to be 100% recyclable. Recycling saves almost 95% of the energy needed to produce the prime aluminum from ore and creates only about 5% of the CO_2 emission as the primary production (Ref 7-9).

Aluminum cast alloys usually contain a certain amount of Si, Cu, Fe, Mn, Mg and Zn that are present either unintentionally, or they are added deliberately to provide special material properties (Ref 3, 10, 11). Iron belongs to common impurities in aluminum cast alloys, but its presence in aluminum cast alloys is the most important because of reducing the adhesion to metal molds (Ref 12). The usage of scrap for the production of aluminum casts leads to increasing amount of iron in the material. Iron is highly soluble in liquid aluminum and its alloys and has a very little solubility in the solid (max. 0.05 wt.%, 0.025 at.%), and this fact leads to the formation of the higher amount of various types of iron-rich intermetallic phases, whose morphology influences the properties of castings (Ref 13-16). In addition, it was suggested that increasing the iron content in the cast Al-Si alloys from 0.1 to 1.4 wt.% resulted in an increase in porosity, particularly the shrinkage porosity, due to the precipitation of long and thick needles (or platelets) of the β-Al_5FeSi phases (Ref 17, 18). Numerous scientific works present some theories about the relationship between the microstructure and quality of castings made from aluminum alloys. Therefore, it is necessary to pay attention to examining the mechanical properties that are significantly affected by microstructure in the secondary aluminum cast alloys, as well. The aim of this study was to assess the quality of the sand castings from the secondary aluminum alloys (which have different amounts of Fe in composition) by different quantitative methods.

2. Experimental Procedure

The AlSi7Mg0.3 aluminum cast alloy bars were produced by the gravity casting technique and casted into the sand mold (Fig. 1) in the company UNEKO Ltd., Zátor, Czech Republic. The experimental bars were made from aluminum scrap. The aim of casting was to produce bars (with dimension 300 × 20 mm—Fig. 1) with different iron contents: the bars produced, according to standard with 0.123 wt.% of Fe (alloy A), with the content of 0.454 wt.% Fe (alloy B) and with the content of 0.655 wt.% Fe (alloy C). The content of Fe was defined by the company with respect to the economic point of

This article is an invited submission to JMEP selected from presentations at the 73rd World Foundry Congress and has been expanded from the original presentation. 73WFC was held in Krakow, Poland, September 23-27, 2018, and was organized by the World Foundry Organization and Polish Foundrymen's Association.

Lenka Kuchariková, Eva Tillová, Milan Uhríčik, Juraj Belan, and **Ivana Švecová**, Department of Materials Engineering, Faculty of Mechanical Engineering, University of Žilina, Univerzitná 8215/1, 010 26 Žilina, Slovakia; and **Michaela Samardžiová**, Advanced Technologies Research Institute, Faculty of Materials Science and Technology in Trnava, Slovak University of Technology in Bratislava, Jána Bottu 2781/25, 917 24 Trnava, Slovakia. Contact e-mail: lenka.kucharikova@fstroj.uniza.sk.

production. The intention was to achieve Fe content as for secondary alloys (with the use of different aluminum scraps) without usage of other technological procedure for affecting the properties or microstructure of castings. The chemical composition of these experimental materials was quantified using spectroscopy analysis on SPECTROMAXx and is given in Table 1.

The samples used for the mechanical test (Fig. 2) were made from casted bars (Fig. 1) by the turning and milling operations. Mechanical properties—ultimate tensile strength (UTS), 0.2% offset yield strength (YS) and elongation changes—were measured on the INSTRON Model 5985 testing machine according to the ISO 6892-1:2009 standard. Test rates and control are set according to the Method A recommended ranges. The Brinell hardness measurement was performed on the Brinell equipment according to the STN EN ISO 6506:2015 standards—1 with 5 mm diameter of the Brinell indenter, loading 5451.75 N and dwell time 15 s. Six samples from each alloy (A, B, C) for mechanical tests were used for measuring.

The metallography observations of microstructure changes, due to the effect of increasing the Fe content, were done by using an optical microscope. The samples were prepared by standard metallographic procedures (wet-ground on SiC papers, DP-polished with 3-μm diamond pastes, followed by Struers Op-S, etched by H_2SO_4 (for better identification of the Fe-rich needlelike intermetallic phases) and Dix-Keller). For the quantitative analysis of size and number of phases, the NIS Elements software with camera Nikon digital sight DS-U2 was used. The type of intermetallic phases was observed using the Thermo-Calc methods, energy-dispersive x-ray (EDX) analysis on a scanning electron microscope (SEM) and morphology assessment on the optical microscope.

Assessment of porosity changes was done using the image analysis software NIS Elements with camera Nikon digital sight DS-U2 and computed tomography (CT) on equipment ZEISS METROTOM OS 2.8.13280.0 with software VG Studio MAX 3.0.1. Results represent the assessment of each product from the secondary aluminum alloys, while assessment by the NIS Elements represents the 2D technology of measuring porosity at about 60 different pores in metallographic cut and the CT assessment represents the 3D technology of measuring at about 800 different pores in the whole sample. The pores' size by the CT was measured from 0.15 mm^3 for cleaning the microporosity, which is always present in aluminum materials, and such porosity is non-critical for properties.

3. Experimental Results and Discussion

3.1 Mechanical Properties

The designers seek to minimize the weight of structural components while maintaining the required tolerances in the manufacturing process and the safety of products (Ref 2, 19). However, almost all the damages of products are related to mechanical properties; therefore, the tensile strength, yield strength, ductility and the Brinell hardness were measured. The higher mechanical properties were measured for the alloy with 0.454% of Fe (Table 2). The UTS was higher for about 6.6%, Brinell hardness for 5.5% and elongation for about 31.42% compared to alloy A (chemical composition according to standards with 0.123% of Fe). The YS was about 4.19% lower. The alloy with 0.655% of Fe showed improvement in mechanical properties, too (UTS for about 4.4%, Brinell hardness for about 3.7% and elongation for about 8.72% compared to alloy A). The YS was also about 2.97% lower. Results of mechanical properties point to the fact that the higher amount of Fe in the chemical composition of material does not lead to deterioration in properties. Small decrease was observed only in the YS in contrast to the other research results, reporting that the existence of iron in the alloy slightly increases the yield strength, but significantly reduces the elongation (Ref 20).

The measured values of elongation and the UTS (Fig. 3) are in good agreement with facts that with increase in the UTS the elongation decreases for each experimental alloy. Because the materials for experiments are cast materials, the results vary due to microstructure quality. The porosity and other disturbances in the material caused small variations in mechanical properties results. This diagram also confirmed the higher mechanical properties for alloy B (with 0.454 wt.% of Fe).

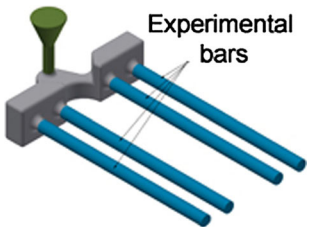

Fig. 1 Model of the sand-casted experimental bars

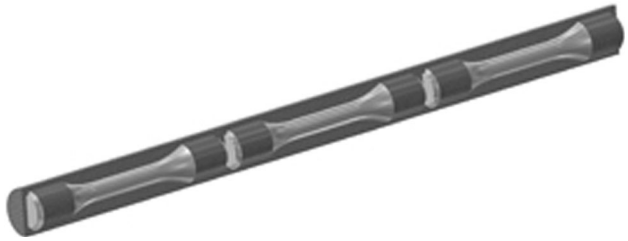

Fig. 2 Model of production of the samples for mechanical test

Table 1 Chemical composition of experimental materials, wt.%

Element	Al	Si	Mg	Fe	Cu	Mn	Zn	Ti
Alloy A	92.253	7.028	0.354	0.123	0.013	0.009	0.036	0.123
Alloy B	91.673	7.340	0.302	0.454	0.021	0.009	0.020	0.118
Alloy C	91.486	7.315	0.292	0.655	0.030	0.010	0.028	0.120

Table 2 Mechanical properties of experimental alloys

Properties	UTS, MPa	YS, MPa	Elongation, %	Brinell hardness HBW 5/250/15
Alloy A	141	101	1.45	52
Alloy B	150	97	1.91	55
Alloy C	147	98	1.58	54

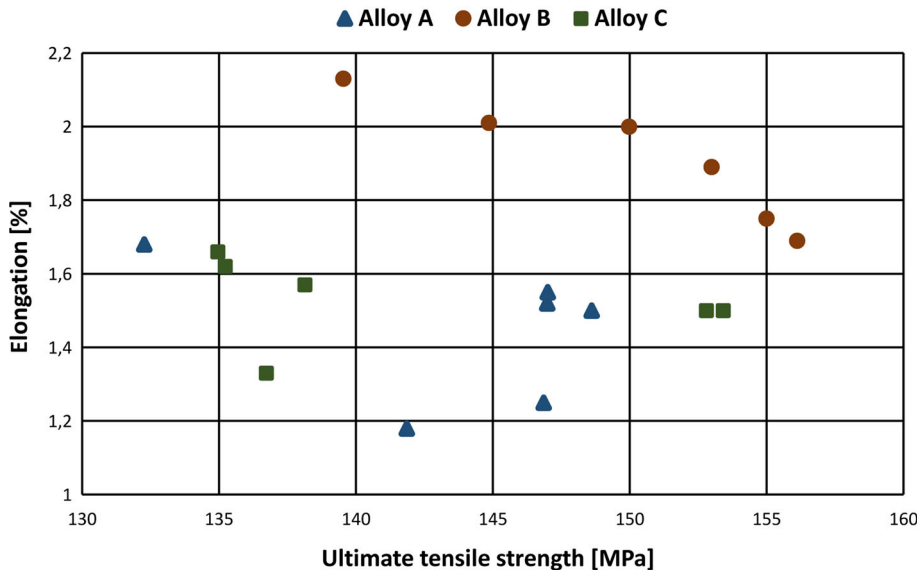

Fig. 3 Relationship between elongation and ultimate tensile strength of experimental alloys

3.2 Microstructure Observation

This type of material belongs to the group of aluminum alloys used especially for casting in mechanical and electrical engineering and automotive and aerospace industries (Ref 18). Therefore, the high quality of castings and excellent mechanical properties of such materials are necessary. The experimental materials were not modified or heat-treated in order to examine the effect of Fe content, especially on microstructure and mechanical properties of the products. These facts reduce production costs of castings.

The microstructure of experimental materials consists of the matrix—dendrites of the α-phase (a solid solution of Si in Al), eutectic phase (a mechanical mixture of eutectic Si and α-phase) and intermetallic phase (Fig. 4). Methods used for the identification of intermetallic phases in the microstructure of experimental materials (Fig. 5) confirmed the occurrence of Fe- and Mg-rich phases: Al_5FeSi (needlelike form), $Al_{15}(FeMg)_2Si_2$ (skeleton-like form), $Al_5Fe_2Mg_2Si_6$ (script-like form) and $Al_8FeMg_3Si_6$ (script-like form).

3.3 2D Quantitative Assessment by NIS Elements

The quantitative assessment (Fig. 6) was focused on area size, length, amount (area fraction in %) of porosity and the Fe-rich intermetallic phases in the needlelike form, due to the fact that nucleation of the Fe-rich phase increases based on oxide films or porosity in castings.

The higher content of iron in alloys B (0.454% of Fe) and C (0.655% of Fe) demonstrated a higher amount of the iron-rich intermetallic phases of group β (AlFeSi—needlelike form) rather than that of group α (Al(FeMn)Si—skeleton-like form) (Fig. 4, 6). Image analysis assessment also confirms that the alloy A has a very small average length of the Fe-rich needles (30.04 μm) in comparison with the other alloys (B = 59.77 μm, C = 52.57 μm). The area fraction increases with increase in the Fe content: alloy A for 1%, alloy B for 2.3% and alloy C for 2.6%. These results confirm the fact that with increasing content of iron (in composition), length and amount of the Fe-rich phases in the form of needles are increasing, as well.

Results of the Fe content effect on the porosity formation in experimental materials show changes (Table 3) and are comparable to research works (Ref 13, 21) which have reported that porosity content increases with iron content. These researches (Ref 13, 21) also show that an increase in the Fe content resulted in a significant increase in the area size of porosity. However, results of area size of pores increases in alloy B showed a decrease in length by about 6.7% and in alloy C an increase by about 13% compared to alloy A. These results demonstrated that material with the highest length of the Fe-rich phases in the form of needles caused formation of the smallest pores in microstructure, but their amount (area fraction) has increased. The volume fraction of pores increased in alloy B (0.454% of Fe) for

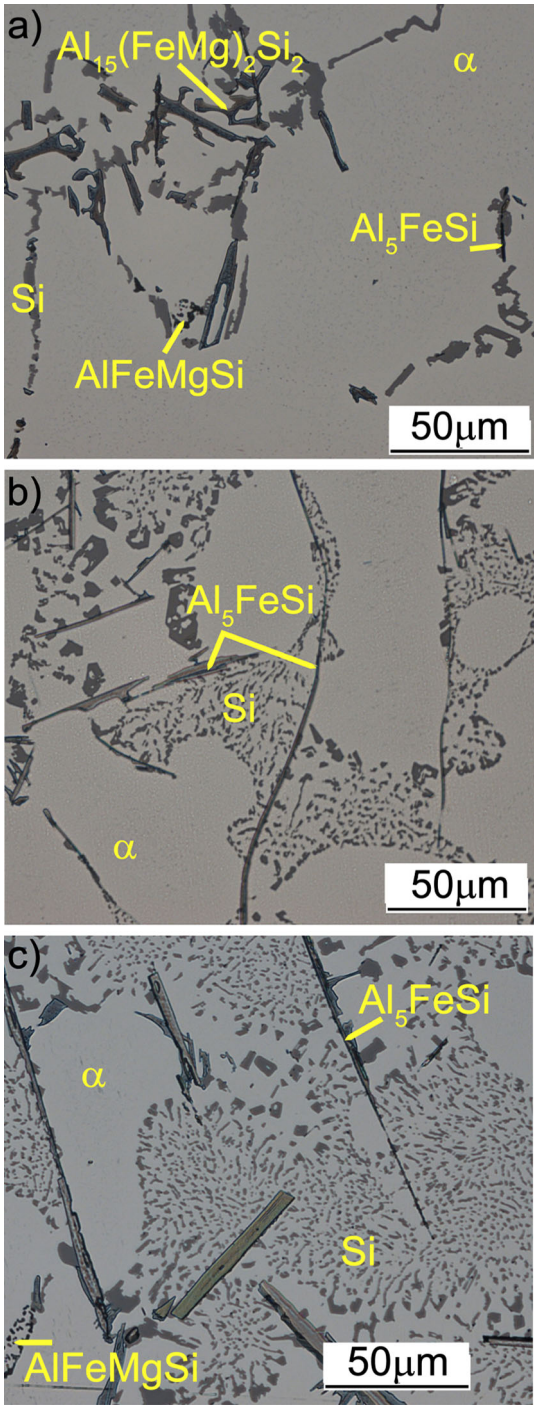

Fig. 4 Microstructure of experimental materials, optical microscope etch. H_2SO_4, (a) alloy A; (b) alloy B; (c) alloy C

about 12.5% and in alloy C (0.655% of Fe) for about 43.8% compared to alloy A.

Results of the volume fraction are comparable to research works (Ref 13, 21); however, the results of area size evaluation are different and the fact that with an increase in the Fe content the pore size area increases as well cannot be confirmed.

3.4 3D Quantitative Assessment by the CT

The CT analysis belongs to nondestructive analysis of manufactured parts which can be used for application after evaluation (Ref 22). This assessment shows influence of the casting technology or content of Fe on porosity formation (Fig. 7). The CT assessment shows that samples made from one bar have different amounts and distribution of porosity (Fig. 7—especially alloy B, C, Table 4). Evaluation by software VG Studio MAX 3.0.1 also confirmed that samples with the middle content of Fe (alloy B = 0.454%) have the smallest diameter, surface and volume of porosity compared to the other two alloys (A, C) (Table 4). The differences (in alloy B) were 6% smaller in diameter, for about 17% smaller in volume and for about 14% smaller in surface of porosity compared to alloy A.

The higher content of Fe (alloy C = 0.655%) has by about 3% smaller diameter, 8% lower volume and 5% lower surfaces compared to alloy A. The comparisons of the material B (0.454% of Fe) and C (0.655% of Fe) (materials with higher amounts of Fe) demonstrated that increasing content of Fe caused formation of larger and numerous porosity in the microstructure.

The CT analysis results demonstrated that material B has the smallest porosity of all the alloys, and therefore the mechanical properties have the highest values for these experimental alloys. These results confirm the results of du Plessis (Ref 23) who reported in his research work: "porosity has been directly linked to mechanical performance of the parts and the area fraction of pores in the fracture surfaces correlates well with the ductility and strength, with more porosity decreasing both the ductility and strength in Al-Si-Mg cast alloy."

The comparison of the 2D and 3D analyses of the Fe-rich phases in the form of needles and porosity is shown in Fig. 8. The quantitative analysis results confirm that material with the highest length of Fe-rich phases in the form of needles (alloy B) has the smallest surface of pores (measured by the CT analysis) and area size of pores (measured by the image analysis), and therefore the mechanical properties are the best (Table 2). Despite the presence of higher content of Fe in the needlelike intermetallic phases, the material B has a very good elongation with the UTS (Fig. 3and Table 2). These results confirm that the length of the Fe-rich needles is not critical for properties of aluminum alloys, but the size of porosity is (Fig. 8). The size of porosity is probably related to increasing amount (area fraction) of the Fe-rich needles (Fig. 8).

4. Conclusions

The quality assessment of the sand Al castings microstructure confirmed that the higher Fe content mostly leads to the formation of the needlelike Fe intermetallic phases with growing length and area fraction. It was also confirmed that increasing content of Fe leads to increasing area fraction of the Fe-rich needles, but the size of these phases was not concurrently increasing with increasing content of Fe.

The porosity formation was different for alloys with an increasing amount of Fe. The 2D and the 3D quantitative

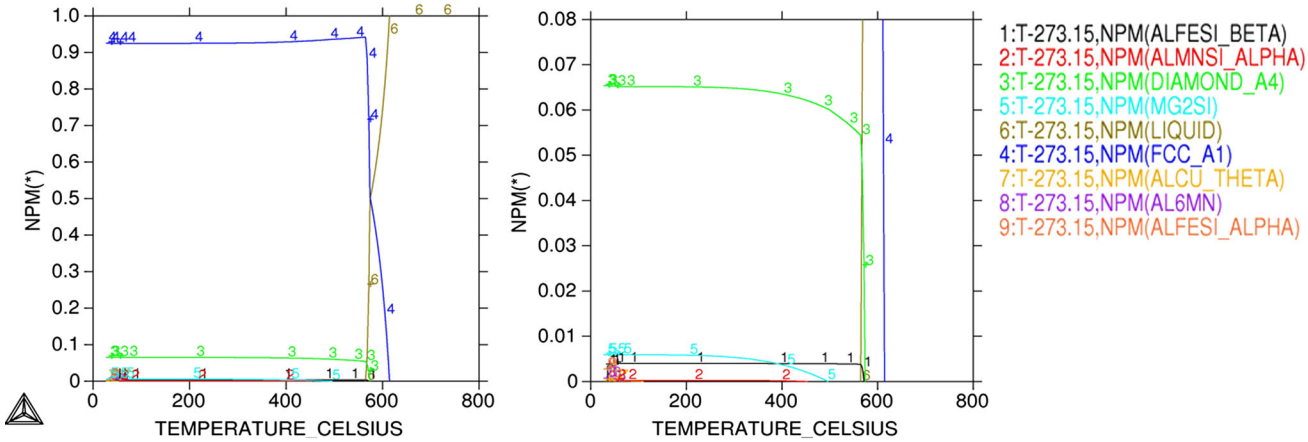

(a)

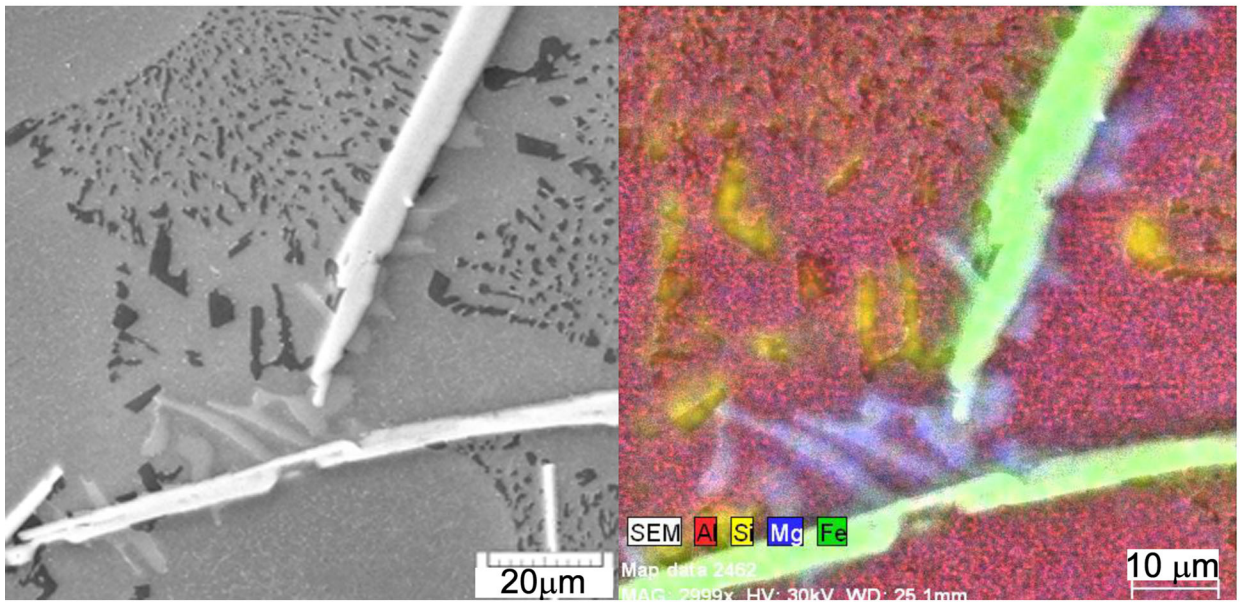

(b)

Fig. 5 Methods for the identification of intermetallic phases in the microstructure of experimental materials. (a) Thermo-Calc; (b) SEM observation with EDX analysis

evaluations show that the lowest area size of porosity is in the material with a middle amount of Fe (0.454 wt.%), while this material has the largest length of the Fe-rich needlelike intermetallic phases. In addition, this material has the highest mechanical properties compared to alloys A and C. These facts relate to the work of Cao and Campbell (Ref 17). They observed that "the fracture of the casting was not caused by the brittleness of the Fe-rich phases (β-Al_5FeSi) but the cracks were actually double oxide films, which had the Fe-rich phases nucleated on their wet sides. This results in decreasing the mechanical properties of the casting, due to the interaction between a double oxide film and the Fe-rich phase."

Material with the highest amount of Fe (alloy C = 0.655 wt.%) has the smallest length but higher amount of the Fe-rich needles than alloy B and the largest pore size and area fraction; therefore, the mechanical properties show lower values.

The results confirm that mechanical properties are more affected by porosity and not by the length of the Fe-rich phases. In addition, measured amount of the Fe-rich phases in needlelike form is significant (increases with increasing content of iron), which may act as nucleation sites for porosity formation. Therefore, the material with the highest content of Fe has the highest amount of porosity.

These studies confirm that materials with the higher Fe content, without affecting the formation of the Fe-rich needles

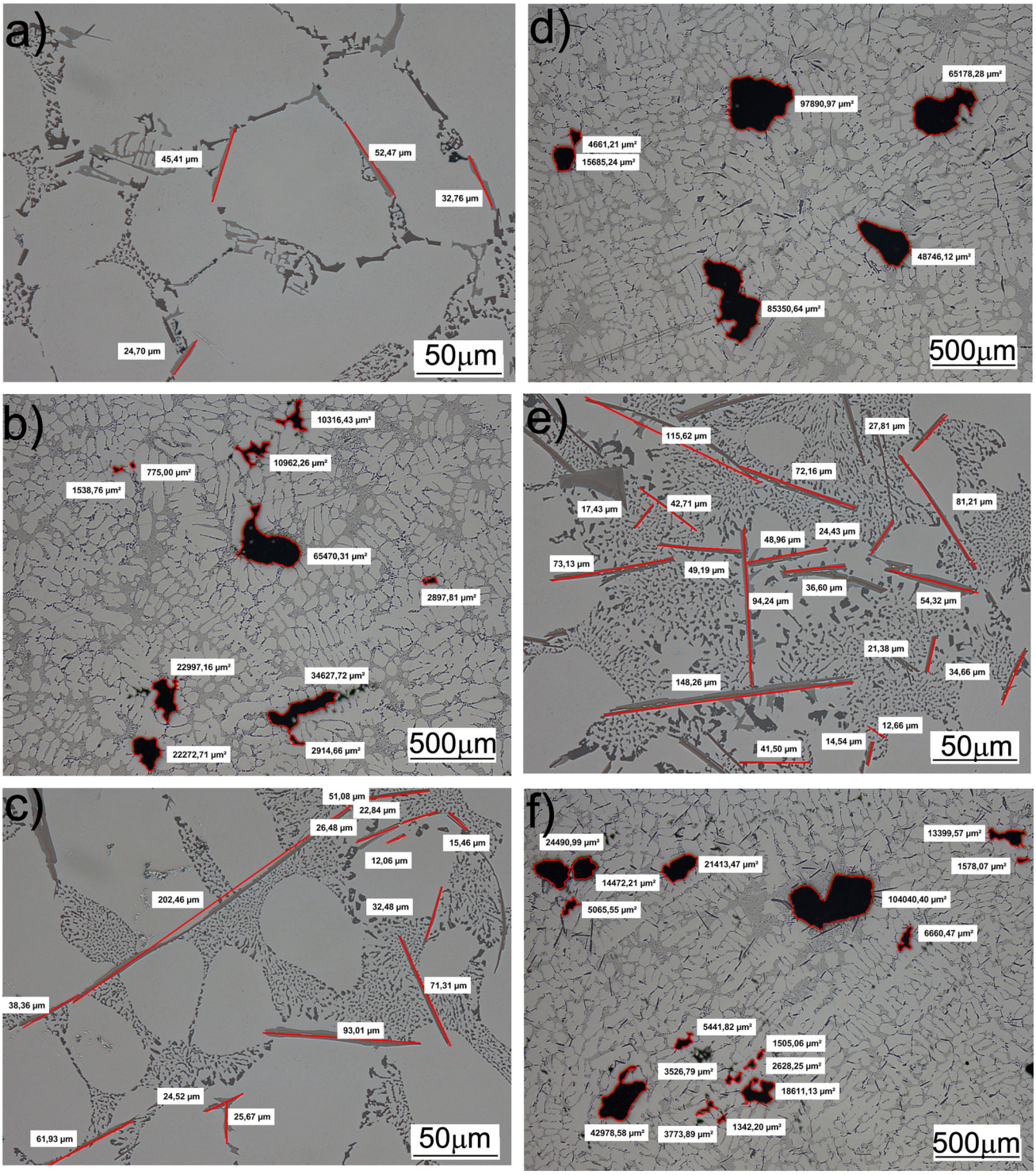

Fig. 6 2D quantitative analysis of length of Fe-rich phases and area size of porosity, optical microscope etch. Dix-Keller. (a), (b) alloy A; (c), (d) alloy B; (e), (f) alloy C

Table 3 Results of the porosity quantitative analysis

Alloys	A	B	C
Area size of pores, μm^2	$20208^{\pm 0.9}$	$18937^{\pm 0.14}$	$22833^{\pm 0.3}$
Volume fraction of pores, %	$1.6^{\pm 0.02}$	$1.8^{\pm 0.01}$	$2.3^{\pm 0.01}$

intermetallic phases with other technologies, are not so unsafe and can be used as materials for aluminum castings. The alloy B has better properties than the material with the Fe content according to standards (alloy A), and the alloy C has comparable properties with alloy A. The question is the amount over the 0.454 up to 0.655 wt.% of Fe. Therefore, it is necessary to clarify up to what percentage of Fe in the

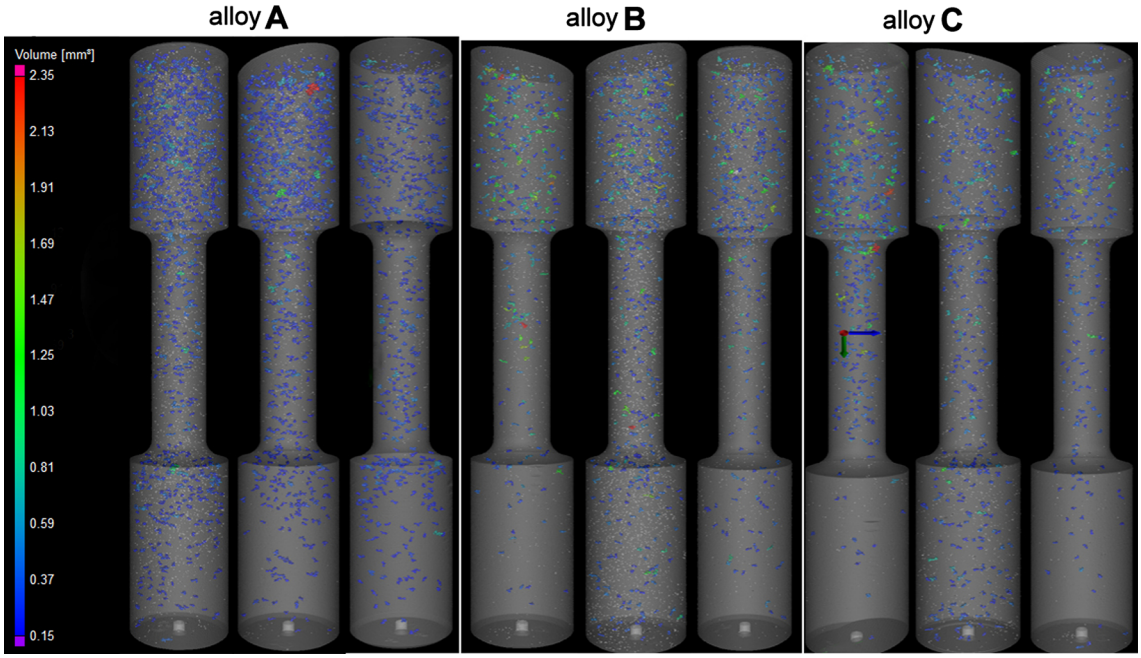

Fig. 7 CT assessment of volume distribution of pores in experimental alloys and its quantitative analysis in experimental alloys

Table 4 Results of the CT porosity analysis in experimental alloys

Alloys	Samples	Diameter, mm	Volume, mm^3	Surface, mm^2
A	1	$1.47^{\pm0.002}$	$0.233^{\pm0.002}$	$4.512^{\pm0.002}$
	2	$1.50^{\pm0.004}$	$0.228^{\pm0.001}$	$4.665^{\pm0.001}$
	3	$1.55^{\pm0.003}$	$0.226^{\pm0.002}$	$4.843^{\pm0.002}$
B	1	$1.47^{\pm0.002}$	$0.192^{\pm0.002}$	$4.142^{\pm0.002}$
	2	$1.36^{\pm0.001}$	$0.191^{\pm0.002}$	$3.832^{\pm0.002}$
	3	$1.42^{\pm0.002}$	$0.188^{\pm0.001}$	$4.005^{\pm0.002}$
C	1	$1.51^{\pm0.002}$	$0.225^{\pm0.002}$	$4.751^{\pm0.001}$
	2	$1.44^{\pm0.002}$	$0.205^{\pm0.002}$	$4.253^{\pm0.002}$
	3	$1.43^{\pm0.004}$	$0.202^{\pm0.003}$	$4.334^{\pm0.001}$

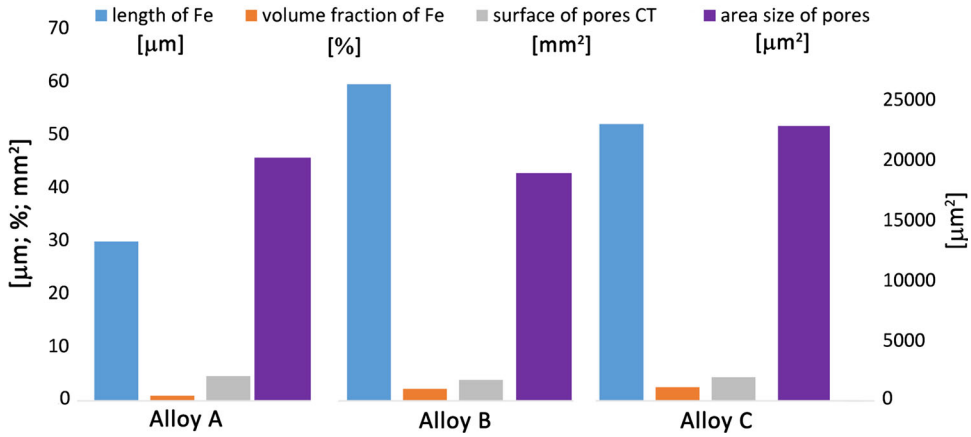

Fig. 8 Comparison of image analysis and CT analysis

secondary aluminum cats alloys are these materials suitable for industrial applications.

Acknowledgments

The authors acknowledge the projects VEGA N°1/0533/15 and KEGA 049ŽU-4/2017 for the financial support of this work.

References

1. K.A. Shriwas and C.V. Kale, Impact of Aluminum Alloys and Microstructures on Engineering Properties—Review, *J. Mech. Civ. Eng.*, 2016, **13**(3), p 16–22
2. Q. Liu, S. Chen, R. Gu, W. Wang, and X. Wei, Effect of Heat Treatment Conditions on Mechanical Properties and Precipitates in Sheet Metal Hot Stamping of 7075 Aluminum Alloy, *J. Mater. Eng. Perform.*, 2018, **27**(9), p 4423–4436
3. F. Grosselle, G. Timelli, and F. Bonollo, Doe Applied to Microstructural and Mechanical Properties of Al-Si-Cu-Mg Casting Alloys for Automotive Applications, *Mater. Sci. Eng. A*, 2010, **527**, p 3536–3545
4. R.X. Li, R.D. Li, L.Z. He, C.X. Li, H.R. Gruan, and Z.Q. Huet, Age Hardening Behavior of Cast Al-Si Base Alloy, *Mater. Lett.*, 2004, **58**, p 2096–2101
5. S.G. Irizalp and N. Saklakoglu, Effect of Fe-Rich Intermetallic on the Microstructure and Mechanical Properties of Thixoformed A380 Aluminum Alloy, *Eng. Sci. Technol. Int. J.*, 2014, **17**(2), p 58–62
6. F. Nový, M. Janecek, and R. Kral, Microstructure Changes in a 2618 Aluminum Alloy During Ageing and Creep, *J. Alloys Compd.*, 2009, **487**(1–2), p 146–151
7. M. Slagsvold, "Effect of Fe and Si Content in Aluminum Alloys as a Result of Increased Recycling," Ph.D. thesis, Norwegian University of Science and Technology, 2011
8. S.K. Das, Designing Aluminum Alloys for a Recycling Friendly World, *Mater. Sci. Forum*, 2006, **519–521**, p 1239–1244
9. L. Senčáková and E. Virčíková, Life Cycle Assessment of Primary Aluminum Production, *Acta Metall. Slovaca*, 2007, **13**(3), p 412–419
10. C.T. Rios, R. Caram, C. Bolfarini, F.W.J. Botta, and C.S. Kiminami, Intermetallic Compounds in the Al-Si-Cu System, *Acta Microsc.*, 2003, **12**, p 77–82
11. R.S. Rana, R. Purohit, and S. Das, Reviews on the Influences of Alloying elements on the Microstructure and Mechanical Properties of Aluminum Alloys and Aluminum Alloy Composites, *Int. J. Sci. Res. Publ.*, 2012, **2**(6), p 1–7
12. M. Tupaj, A.W. Orłowicz, M. Mróz, A. Trytek, and O. Markowska, The Effect of Cooling Rate on Properties of Intermetallic Phase in a Complex Al-Si Alloy, *Arch. Foundry Eng.*, 2016, **16**(3), p 125–128
13. J.A. Taylor, Iron-Containing Intermetallic Phases in Al-Si Based Casting Alloys, *Procedia Mater. Sci.*, 2012, **1**, p 19–33
14. A. Bjurenstedt, S. Seifeddine, and A.E.W. Jarfors, The Effects of Fe-Particles on the Tensile Properties of Al-Si-Cu Alloys, *Metals*, 2016, **6**, p 314–329
15. K.K. Pius, "A Study on the Effects of Iron on Microstructure and Mechanical Properties of Aluminum-Silicon Alloys," Master thesis, University of Nairobi, 2012
16. X. Fang, G. Shao, Y.Q. Liu, and Z. Fan, Effect of Intensive Forced Melt Convection on the Mechanical Properties of Fe Containing Al-Si Based Alloys, *Mater. Sci. Eng. A*, 2007, **445–446**, p 65–72
17. X. Cao and J. Campbell, The solidification characteristics of Fe-rich intermetallics in Al-11.5Si-0.4Mg cast alloys, *Metall. Mater. Trans. A*, 2004, **35A**, p 1425–1435
18. K. Bangyikhan, "Effects of Oxide Film, Fe-Rich Phase, Porosity and Their Interactions on Tensile Properties of Cast Al-Si-Mg Alloys," Ph.D. thesis, University of Birmingham, 2005
19. K.O. Pedersen, H.J. Roven, O.G. Lademo, and O.S. Hopperstad, Strength and Ductility of Aluminum Alloy AA7030, *Mater. Sci. Eng. A*, 2008, **473**, p 81–89
20. S. Ji, W. Yang, F. Gao, D. Watson, and Z. Fan, Effect of Iron on the Microstructure and Mechanical Property of Al-Mg-Si-Mn and Al-Mg-Si Diecast Alloys, *Mater. Sci. Eng. A*, 2013, **564**, p 130–139
21. M.O. Otte et al., Controlling Porosity-Related Casting Rejects: Understanding the Role of Iron in Al-Si Alloys, *Trans. Am. Foundrymen's Soc.*, 1999, **107**, p 471–478
22. A. du Plessis et al., Standard Method for microCT-Based Additive Manufacturing Quality Control 1: Porosity Analysis, *MethodsX*, 2018, **5**, p 1102–1110
23. A. du Plessis et al., Prediction of mechanical performance of Ti6Al4V cast alloy based on microCT-based load simulation, *J. Alloys Compd.*, 2017, **724**, p 267–274